Communications in Physics, Vol. 34, No. 4 (2024), pp. 399-412

DOI: https://doi.org/10.15625/0868-3166/21246

Enhancement of photocatalytic characteristics of Ag-Cu₂O nanocomposites synthesized via one-pot method for polluted water treatment

Dao Phi Hung 1,2 , Nguyen Tien Dung 3 , Nguyen Thuy Chinh 1,2 , Trinh Thanh Huyen 3 , Vu Dinh Hieu 1 and Thai Hoang 1,2,†

E-mail: †hoangth@itt.vast.vn

Received 31 July 2024; Accepted for publication 9 December 2024; Published 15 December 2024

Abstract. The paper presents results on the synthesis of Ag-Cu₂O nanocomposites by one pot method. The characteristics, properties of Ag-Cu₂O nanocomposites were determined using X ray diffraction, Field Emission Scanning Electron Microscopy (FESEM) and UV-Vis diffuse reflectance spectroscopy. The obtained results indicated that the crystalline size of Cu₂O particles was approximately 38.36 nm while that of Ag particles was about 12 nm. The FESEM images showed a tendency for agglomeration of Cu₂O particles. The Ag nanoparticles were dispersed regularly on the surface of Cu₂O particles. Due to modification with AgNO₃ salt solution, the Ag-Cu₂O nanocomposites exhibited a better ability to absorb light than the Cu₂O particles and had a lower bandgap energy. Additionally, the Ag-Cu₂O nanocomposites also had a higher photocatalytic activity than that of the Cu₂O particles. The Ag-Cu₂O nanocomposite is promising for water treatment applications.

Keywords: Ag-Cu₂O; methylene blue; nanocomposite; photocatalytic performance.

Classification numbers: 81.05.-t; 82.80.-d.

1. Introduction

The rapid growth of population and industrialization has caused severe environmental pollution, serious influence on human life and the ecosystem [1]. Several methods have been employed for pollution treatment, including physical, biological, and chemical methods. However,

©2024 Vietnam Academy of Science and Technology

¹Institute for Tropical Technology, Vietnam Academy of Science and Technology, 18 Hoang Quoc Viet, Cau Giay, Hanoi, Vietnam

²Graduate University of Science and Technology, Vietnam Academy of Science and Technology, 18 Hoang Quoc Viet, Cau Giay, Hanoi, Vietnam

³Falcuty of Chemistry, Hanoi National University of Education, 136 Xuan Thuy, Cau Giay, Hanoi, Vietnam

these methods are expensive, can generate toxic byproducts, and have limited effectiveness. Therefore, there is urgent for the development of highly effective and environmentally friendly methods to treat environmental pollutions. One promising solution is the use of nanomaterials, nanohybrid materials, nanocomposites based on inorganic oxides and inorganic compounds such as Ag-Ti₂O [2], TiO₂-Cu₂O [3], Cu-Cu₂O [4], Ag-ZnO [5], zeolite/Ag-Zn [6], ZnO/graphene oxide [7] due to their unique physicochemical properties.

The synthesis of Ag-Cu₂O nanocomposites can be achieved through several methods, including chemical reduction, sol-gel, hydrothermal, electron-beam and microwave-assisted methods [8]. The Ag-Cu₂O nanocomposites have several potential applications in pollution treatment. One of the most promising applications is the treatment of water pollutants [8, 10]. The Ag-Cu₂O nanocomposites can be used to degrade organic pollutants by photocatalytic activity under visible light, such as dyes and pharmaceuticals in water. Yan et al. demonstrated that the photocatalytic effect of Ag-Cu₂O composites is stronger than that of the Ag and Cu₂O particles (Cu₂O NPs) [11]. The authors argue that the enhanced photocatalytic activity of the Ag-Cu₂O material is due to the Schottky barrier effect. The Ag nanoparticles (AgNPs) on surface of Cu₂O NPs act as electron reservoirs when electrons from the conduction band return to the valence band due to the Schottky effect formed between the contact surfaces of AgNPs and Cu₂O NPs. This prevents the recombination of photo-generated electrons and holes [12]. Additionally, the Cu₂O NPs is a semiconductor material, and when combined with AgNPs, they can enhance the surface-enhanced Raman scattering (SERS) effect [8]. Both the AgNPs and Cu₂O NPs have good antibacterial activity, especially in nano scale [8]. When AgNPs and Cu₂O NPs were combined in a nanostructured composite material, their synergistic effect could increase the antibacterial activity of material.

The Ag-Cu₂O composites exhibit many distinctive characteristics and properties such as SERS capability, catalytic activity, and strong and long-lasting antibacterial performance. Therefore, their fabrication has become a research direction that receives significant attention from experts and scientists. However, existing studies have mainly focused on the synthesis of Ag-Cu₂O composites using various methods and individual applications such as catalytic activity and antibacterial properties. Now, synthesis of Ag-Cu₂O materials using a simple method for applications in treating wastewater containing pollutants such as organic matter and bacteria have scientific, practical, and topical significance. The purposes of this work are to synthesis of Ag-Cu₂O composites by a simple one-step method, discussion, and evaluation their characteristics, properties.

2. Experiment

2.1. Materials

In this work, some chemicals were used such as CuSO_{4.}5H₂O, AgNO₃ salts, NaOH, ascorbic acid, methylene blue (MB) were supplied by Sigma-Aldrich (USA).

2.2. Sample preparation

Preparation of Cu_2O NPs: Firstly, 10 g of $CuSO_4.5H_2O$ salt, corresponding to 0.04 mol were dissolved in 30 ml of distilled water to obtain solution A. Then, 3.2 g of NaOH were dissolved in 30 ml of distilled water to obtain solution B. The solution B was slowly added to the solution A with stirring for 20 minutes until the reaction was complete. Next, 3.52 g of ascorbic acid was dissolved in 30 ml of distilled water to obtain solution C. The solution C was then added to the

mixture of solution A and solution B and allowed to react completely for 1 hour. After that, the upper layer of solution was removed by decantation, and the solid precipitate were washed by acetone three times. This solid was then dried in a vacuum oven at 40 °C to obtain Cu₂O NPs.

Dao Phi Hung et al.

Preparation of Ag-Cu₂O NPs: 2 g of Cu₂O NPs were weighed and added to a 200 ml triangular flask containing 50 ml of distilled water. The mixture was stirred ultrasonically using a T10 Ultra-Turrax® digital device (IKA, Germany) at a speed of 6000 rpm for 1 hour. Then, 0.16 g of AgNO₃ salt was dissolved in 10 ml of distilled water, after that the prepared AgNO₃ solution was slowly added to the flask containing the Cu₂O NPs dispersion. The flask was covered with black wrap and stirred for 2 hours on a magnetic stirrer at a speed of 200 rpm. Finally, the resulting material was filtered and sampled, and then dried overnight in a vacuum oven at 50 °C to obtain the Ag-Cu₂O NPs. The composition of the reaction system to prepare Ag-Cu₂O nps and their codes are presented on Table 1.

Code	Cu ₂ O (gram)	Distilled water (gram)	AgNO ₃ (gram)	Weight ratio of Ag/Cu2O
C0	2	-	-	0-1
CA10	2	50	0.32	1-10
CA15	2	50	0.228	1-15
CA20	2	50	0.16	1-20

Table 1. Composition of the reaction system to prepare Ag-Cu₂O nps and their codes.

2.3. Analysis

The characteristics of Cu_2O and $Ag-Cu_2O$ NPs were determined by various methods including: X-ray diffraction (XRD) analysis of the NPs was conducted using a D8-Advance 5005 X-ray diffractometer from Bruker (Germany) with $Cu-K_{\alpha}$ ($\lambda=1.5406$ Å) and a scanning rate of 0.01° /s for crystal structure and phase analysis. The surface morphology of NPs was observed using a FESEM (FESEM S4800) from Hitachi (Japan) with an acceleration voltage of 5 kV at a magnification of 50 k. To enhance electrical conductivity, all samples for FESEM measurement were coated with a very thin layer of Pt. The band gap of NPs was determined by an UV-Vis diffuse reflectance spectroscopy (UV 2600, Shimadzu, Japan), which was equipped with the ISR-2600Plus two-detector integrating sphere, with a wavelength range of 200 nm - 800 nm. The energy dispersive X-ray spectroscopy (EDS) mapping analysis was recorded by Oxford Instruments detector (Ultim Max 65).

2.4. Photocatalytic performance

MB is a toxic substance that can cause cancer, is non-biodegradable, and poses a serious threat to human health and environmental safety. It is often released into natural water sources, becoming a health hazard to humans and living organisms. Thus, there is a need to develop an environmentally friendly and effective technology to remove MB from wastewater [13]. Photocatalytic oxidation is an advanced oxidation process that is widely used to remove MB which exists in the form of a cation in water with a pKa of 3.8. Therefore, when the pH value is between 4 and 8, the surface of the NPs becomes negatively charged, while the cations in MB solution becomes

positively charged, resulting in electrostatic attraction that affects insignificantly on MB treatment process. Hence, the pH value of 7 was chosen in this work.

The experimental conditions for determining MB were carried out as follows: a certain amount of Ag-Cu₂O NPs (with concentrations of 0.8, 1, 1.2, and 1.4 g/L) was dispersed in 100 mL of MB solution (6 ppm, pH = 7). The mixture was stirred for 1 hour in the dark to ensure even distribution of Ag-Cu₂O NPs. Then, the mixture was taken out, stirred and irradiated with a 9 W UV lamp (365 nm wavelength) at a distance of 25 cm from the solution layer at 30 °C using a thermostat bath. The samples were taken at different time intervals. After performing NPs catalyst separation step by centrifugation (at a speed of 9,000 rpm for 5 minutes), the solution was measured using UV-Vis spectroscopy to determine the MB concentration. Continuously, the catalytic activity of Ag-Cu₂O NPs was evaluated.

During the experiment, the MB concentration was determined using UV-Vis spectroscopy (Fig. 1). The calibration curve of MB solution was preparing MB solutions at various concentrations (1-8 ppm) based on absorbance intensity of their UV-Vis spectra (At 665 nm wavelength) (Fig. 2). The linear regression equation of the MB solution at wavelength of 665 nm was: y = 5.163x + 0.3525, where x is the optical density (absorbance), and y is the concentration of the MB solution. The linear regression coefficient R^2 is 0.9986, indicating a high level of agreement with the linear model. Based on the UV-Vis spectra of MB solution before and after irradiation, the concentration of MB solution was determined using the regression equation at the 665 nm wavelength.

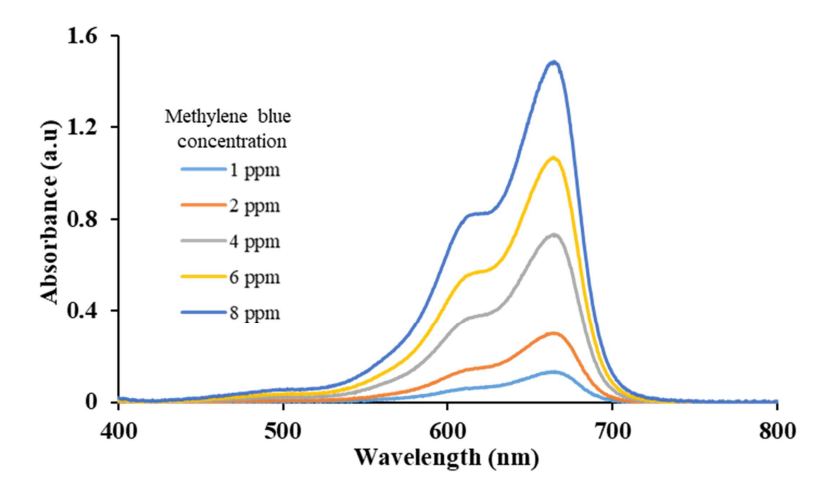


Fig. 1. UV-Vis absorption spectra of MB solutions at different concentrations.

3. Results and discussion

3.1. Characteristics and properties of Cu_2O and $Ag-Cu_2O$ nanoparticles

3.1.1. Ultraviolet-visible (UV-Vis) diffuse reflectance spectroscopy analysis

The UV-Vis diffuse reflectance spectra of Cu_2O and $Ag-Cu_2O$ NPs (with initial mass ratio of Cu_2O NPs /Ag = 15/1 - CA15) are presented in Fig. 3. It is clear that the Cu_2O NPs have better

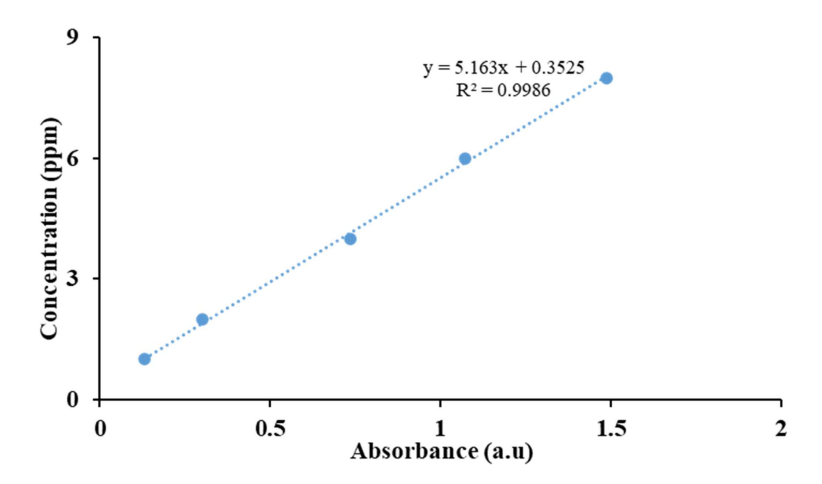


Fig. 2. Calibration curve of MB solution at wavelength of 665 nm

ability to reflect light in the range of 200 - 800 nm than the Ag-Cu₂O NPs. This means that the light absorption ability of Ag-Cu₂O NPs is higher than that of the unmodified Cu₂O NPs.

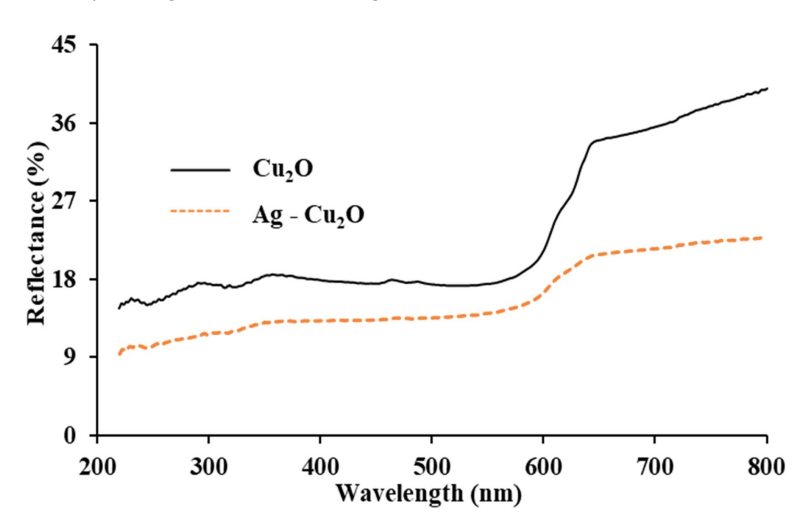


Fig. 3. UV-Vis diffuse reflectance spectra of Cu₂O and Ag-Cu₂O NPs.

As it is known that the Cu₂O and Ag-Cu₂O exhibit direct band gaps [12]. Thus, the energy bandgap of the materials can be determined from its UV-Vis spectra using the formula: $(\alpha h v)^2$ = A(hv - E_g) where h, A, E_g and v are respectively the Planck constant, a constant, the energy of the bandgap and frequency of light while α is the absorption coefficient calculated using the formula F(R) = $(1-R)^2/2R = \alpha$, with R is the reflection coefficient [7]. The tangent line to the curve intersects the horizontal axis at the point where the E_g is located. The graph of $[F(R)hv]^2$ versus hv for Cu₂O and Ag-Cu₂O NPs is displayed in Fig. 4. The E_g of Cu₂O and Ag-Cu₂O NPs were determined to be 1.81 eV and 1.58 eV, respectively. It can be seen that after decorating

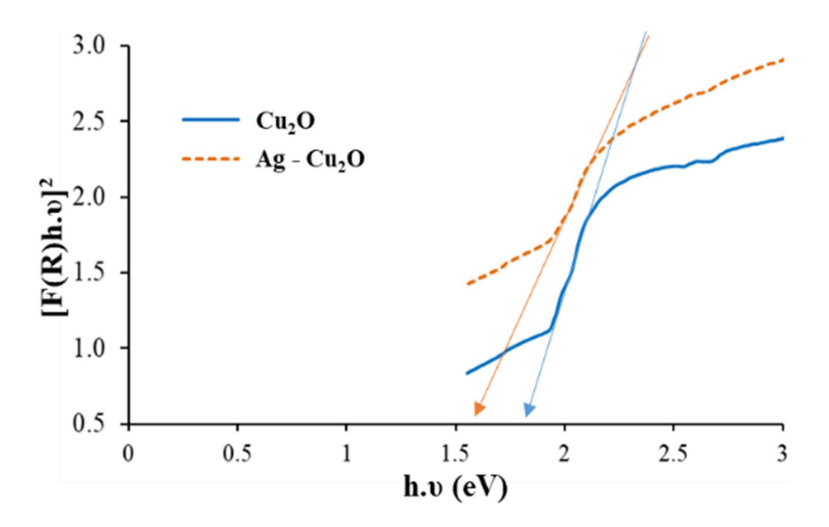


Fig. 4. Relationship between $F(R)h.v^2$ and value of h.v of Cu_2O and $Ag-Cu_2O$ NPs.

AgNPs onto the Cu_2O NPs, the E_g of Ag- Cu_2O NPs decreases. There are some main reasons of this effect.. Firstly, it may be electronic interation between Ag and Cu_2O NPs. The AgNPs are rich in free electrons that can easily resonate with the electrons in the conduction band of Cu_2O NPs. Therefore, when stimulated by light, electrons can easily transfer from the valence band to the conduction band, contributing to the reduction of the E_g of Cu_2O NPs. An other reason may be that Ag NPs exhibit surface plasmon resonance, where their conduction electrons oscillate collectively under light stimulation. This plasmonic effect can couple with the electronic states of Cu_2O , resulting in a reduction of the effective E_g . The above analysis results show that the Ag- Cu_2O NPs have higher light absorption ability and a reduced energy band gap compared to the original Cu_2O NPs. Therefore, the photocatalytic activity of the Ag- Cu_2O NPs is improved.

3.1.2. X-ray diffraction (XRD) analysis

The XRD patterns of Cu₂O and Ag - Cu₂O NPs are performed in Fig. 5.

It is clear that the XRD pattern of Cu_2O NPs exhibits characteristic diffraction peaks at 2θ angles of 30°, 36°, 43°, 61°, 74°, and 77°, corresponding to the (110), (111), (200), (220), (311), and (222) lattice planes of the cuprite crystal structure of Cu_2O . In contrast, the XRD pattern of the Ag-Cu₂O NPs indicates additional diffraction peaks of AgNPs at 2θ angles of 38.20°, 44.40°, and 64.60°. These diffraction peaks correspond to the (111), (200), and (220) crystal planes of AgNPs. The crystal planes match the standard diffraction peaks of AgNPs with a face-centered cubic structure. This shows that the Ag crystals have successfully been deposited on the surface of Cu_2O crystals, in other words, the Cu_2O NPs have been successfully modified by AgNPs.

From the XRD patterns, the average crystalline grains size of materials can be calculated using the Debye-Scherrer formula (assuming that the crystal size is small enough to exhibit the broadening effect of XRD):

$$D = \frac{0.9\lambda}{\beta\cos\theta},$$

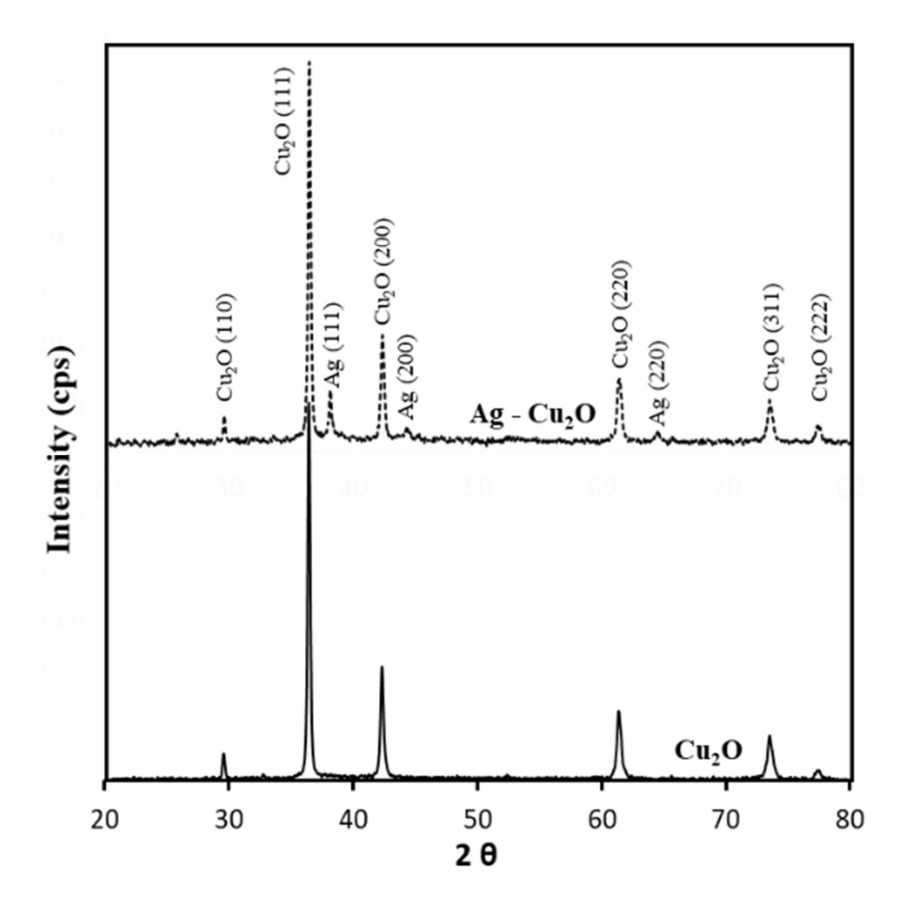


Fig. 5. XRD patterns of Cu₂O and Ag - Cu₂O NPs.

where D is the average crystal size (nm), λ is the wavelength of X-rays (in this case $\lambda = 1.5406 \text{ Å}$). β is the full width at half maximum of the diffraction peak (rad) and θ is the Bragg angle.

For Cu₂O: the size of the grain corresponding to (111) plane ($\beta = 0.0864$, $\theta = 77^{\circ}$) is found to be of 38.36 nm

Whereas, for Ag - Cu₂O: the size of the same (111) orientation ($\beta = 0.0886$, $\theta = 64.60^{\circ}$) has a size as small as 12.68 nm.

The analysis results of XRD patterns indicate that the size of the crystalline grains of Cu_2O and Ag - Cu_2O NPs is 38.36 and 12.68 nm, respectively.

3.1.3. Morphology

The FESEM images of Cu₂O and Ag - Cu₂O NPs are seen in Fig. 6.

The FESEM images show that the Cu_2O NPs are in the form of cubic shape and a tendency to agglomerate with an average particle size of about 500 nm. This is a common phenomenon for nanoparticles due to a large surface area-to-volume ratio and surface energy. The nanoparticles are easy to agglomerate under certain condition such as high humidity. This explains a difference in particle size determined by XRD and FESEM methods. After being modified with AgNPs, the Ag

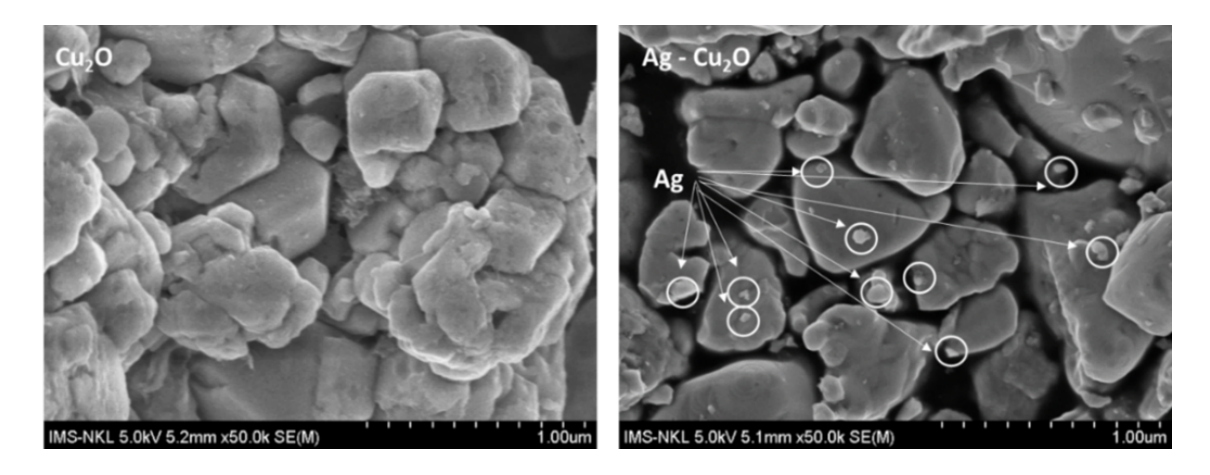


Fig. 6. FESEM images of Cu₂O and Ag - Cu₂O NPs.

crystals are formed on the surface of Cu₂O NPs. The size of AgNPs determined by the FESEM method is much larger than the value of grains measured by the XRD method. This is because AgNPs determined by XRD are crystalline grains, but not the separarted nanoparticles. AgNPs observed in FESEM images can consist of several grains.

3.1.4. Energy dispersive X-ray spectroscopy (EDS) mapping analysis

The EDS and element mapping of $Ag-Cu_2O$ NPs was presented in Fig. 7. The $Ag-Cu_2O$ composite contains three elements: Cu, O, and Ag. The Ag element accounts for 16.9 wt.%. Elemental mapping indicates a uniform distribution of the Ag element on the surface of the Cu_2O particles. This provides strong evidence of the formation of Ag on the Cu_2O particles.

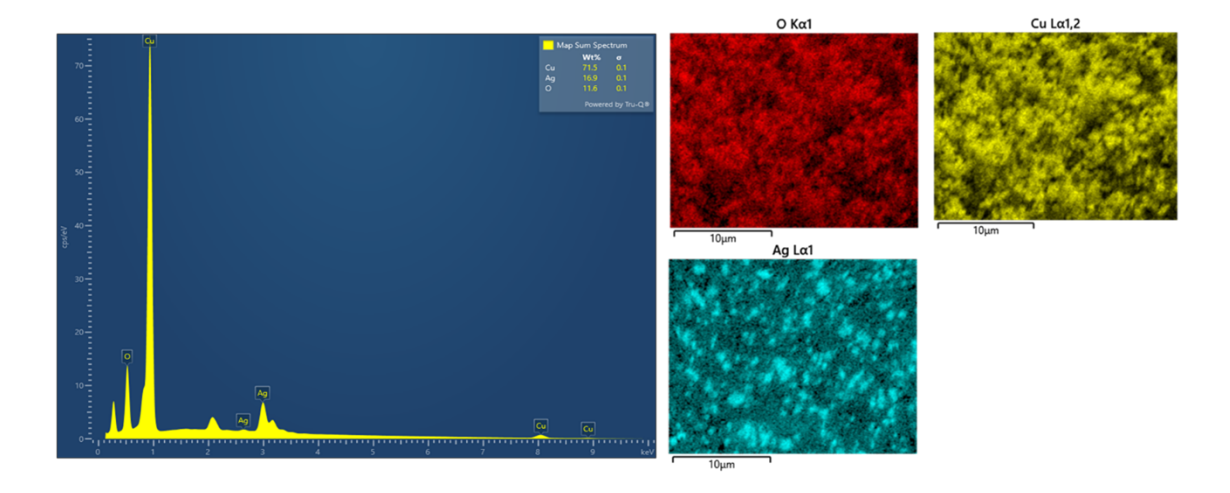


Fig. 7. EDS and element mapping of $Ag - Cu_2O$ NPs.

3.2. Photocatalytic activity of Ag-Cu₂O nanoparticles

3.2.1. Effect of Ag content on photocatalytic activity of Ag-Cu₂O NPs

The methylene blue (MB) degradation efficiency is evaluated by the C/C_0 ratio at different light exposure times, where C is the concentration at time t and C_0 is the initial concentration. A C/C_0 ratio approaching 0 indicates a more efficient degradation process, attributed to the material's high photocatalytic activity. The degradation performance is calculated using the formula: $H = (1 - C/C_0).100\%$. The degradation rate is represented by the rate constant k, and for Ag-Cu₂O NPs, the first-order reaction follows the equation: $\ln(C_0/C) = k.t$, where t is the degradation time. The treatment efficiency of MB by Ag-Cu₂O NPs with varying Ag contents at different UV illumination times is presented in Table 2.

Table 2. Treatment efficiency of MB solution by Ag-Cu₂O NPs under UV illumination at different time intervals.

No	Exposure time	Efficiency of MB treatment (%)			
	(hours)	C0	CA10	CA15	CA20
1	0 (dark store)	11.54	7.58	9.46	11.56
2	2	14.94	16.09	11.38	20.74
3	4	19.40	25.18	15.48	23.62
4	6	21.17	31.37	27.41	25.96
5	8	23.13	37.48	35.33	29.97
6	10	28.04	45.48	57.40	36.42
7	12	30.59	48.72	69.91	40.40

Table 2 shows that keeping MB in the dark leads to a decrease in its concentration. The treatment efficiency of MB by Cu₂O NPs (C0 sample) reaches 11.54%. After 1 hour of ultrasonic vibration and stirring in the dark, the treatment efficiencies for the CA10, CA15, and CA20 NPs are 7.58%, 9.46%, and 11.56%, respectively. Increasing the Ag content in Ag-Cu₂O NPs enhances MB treatment efficiency due to greater adsorption on the NP surfaces, as shown by the CA10 NPs having the lowest efficiency at 7.58%. Conversely, the highest efficiency, achieved by the CA20 NPs, is 11.56%, matching the initial Cu₂O NPs (C0). This effect occurs because AgNPs adhere to Cu₂O NPs, reducing their surface area and thereby decreasing MB contact. Under UV illumination, the ability of Ag-Cu₂O NPs to degrade MB increases rapidly. After 12 hours, the CA15 sample shows the highest treatment efficiency at 69.91%, while the CA20, CA10, and C0 samples achieve efficiencies of 40.40%, 48.72%, and 30.59%, respectively. Thus, Ag-Cu₂O NPs significantly enhance MB degradation compared to Cu₂O NPs alone (30.59%), attributed to their photocatalytic activity as noted in previous research [12]. In addition, the degradation of MB under UV illumination was minimal. After 11 hours of UV exposure using the same UV lamp power of 9W, the degradation efficiency decreased by 2 wt.% [14]. The efficiency of MB degradation under UV illumination is significantly enhanced in the presence of nanoparticles. This serves as evidence for the effectiveness of nanoparticles such as Cu₂O and Ag-Cu₂O nanocomposites in improving degradation performance.

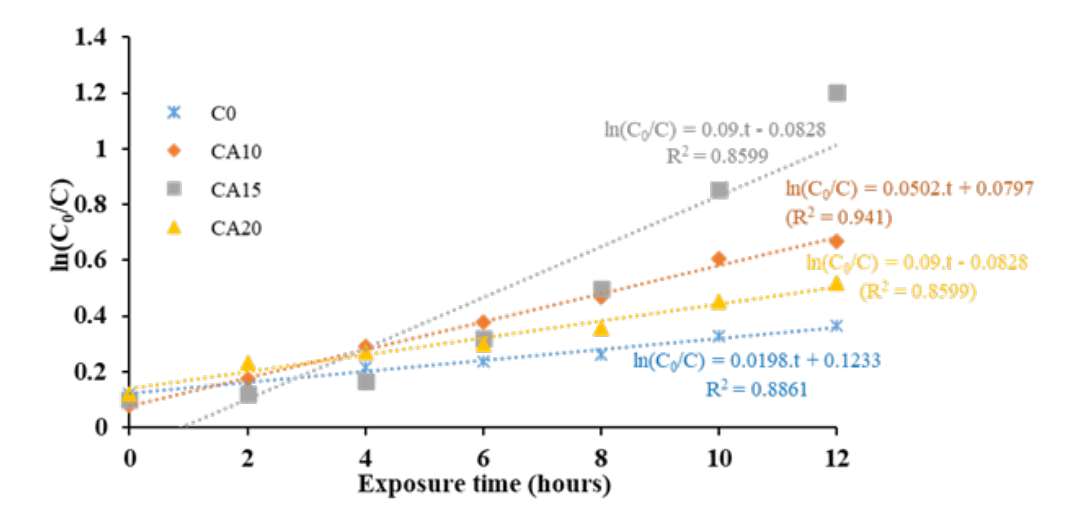


Fig. 8. Graph of relationship between $ln(C_0/C)$ of MB solution using Ag-Cu₂O NPs with various Cu₂O NPs/Ag over time under light exposure.

The Cu_2O NPs modified by Ag are synthesized based on the process of reducing Ag^+ ions by Cu_2O according to following reaction:

$$2~Cu_2O + 4~AgNO_3 \rightarrow 2~Cu(NO_3)_2 + 4~Ag + O_2$$

If the initial Cu_2O NPs/Ag ratio is not optimal, the resulting Ag- Cu_2O NPs may have too little or too much Ag, affecting their photocatalytic activity. This imbalance likely explains why the CA10 and CA20 NPs only slightly outperform the initial Cu_2O NPs (C0). When the ratio is optimal, the surface plasmon resonance of Ag is enhanced with Cu_2O NPs, significantly boosting their photocatalytic efficiency. The kinetics of the MB solution treatment by Ag- Cu_2O NPs with various Cu_2O NPs/Ag ratios were determined using the first-order kinetic equation: $In C_0/C = k.t$ (where k is the degradation rate constant and t is time). The rate constant was calculated from the slope of the $In(C_0/C)$ versus time plot. Fig. 8 presents the relationship between C_0/C for MB solutions treated with Ag- Cu_2O NPs.

The regression coefficients and reaction rate constants for each Ag-Cu₂O NPs photocatalyst were also determined. Except for CA10 NPs, which had a relatively high regression coefficient ($R^2 = 0.941$), other Ag-Cu₂O NPs had regression coefficients below 0.9. This indicates that the linear model of the first-order kinetic reaction equation is suitable for MB decomposition using Ag-Cu₂O NPs with lower Cu₂O NPs/Ag mass ratios. An analysis of the $ln(C_0/C)$ versus UV exposure time graph for CA15 NPs shows that MB decomposition occurs in two stages, each following a different linear kinetic model with a high regression coefficient. Fig. 8 illustrates the relationship between $ln(C_0/C)$ and UV exposure time for MB solutions treated with CA15 NPs, where the initial mass ratio of Cu₂O NPs/Ag is 15/1.

Figure 9 shows that the degradation of the MB solution using CA15 NPs occurs in two distinct stages. In the first stage, the treatment rate is slow, with a rate constant of $k = 0.0355 \, \mathrm{h}^{-1}$ and a kinetic equation of $\ln(C_0/C) = 0.0355t + 0.0706$, yielding a regression coefficient of $R^2 = 0.9645$. During this stage, the Ag-Cu₂O NPs surface is covered by MB, reducing the light contact. As UV illumination continues, the rate increases significantly with a rate constant of $k = 0.1498 \, h^{-1}$ and

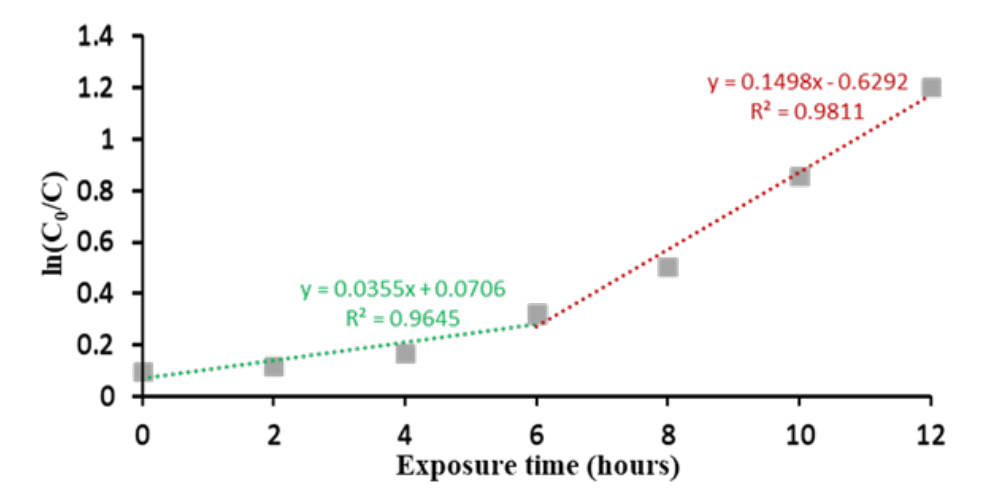


Fig. 9. Relationship between $ln(C_0/C)$ of MB solution using CA15 NPs (initial mass ratio of Cu_2O NPs/Ag of 15/1) and time of UV light exposure.

a kinetic equation of $\ln(C_0/C) = 0.1498t - 0.6292$, resulting in a regression coefficient of $R^2 = 0.9811$. In this second stage, the surface shows little to no MB coverage, enhancing the photocatalytic efficiency. The high regression coefficients ($R^2 > 0.95$) for both stages confirm the suitability of the linear kinetic model. Initially, MB absorbs on the surface, limiting light exposure, thus reducing the treatment rate. Once the MB on the surface is treated, the rate increases. The high $R^2 = 0.9811$ indicates the linear model's validity. The high regression coefficient for CA10 NPs is attributed to the low MB adsorption (just over 5%).

The photocatalytic mechanisms of materials like ZnO, TiO₂, and Cu₂O have been extensively studied [3, 11]. When exposed to UV light, electrons are excited from the valence band (VB) to the conduction band (CB), creating electron-hole pairs in the VB. However, these photogenerated electrons and holes tend to recombine, which reduces the material's photocatalytic activity. Modification of Cu₂O NPs with Ag facilitates the transfer of these photo-generated electrons to Ag, thereby reducing the recombination of electron-hole pairs and enhancing the photocatalytic activity of Cu₂O NPs. For optimal synergistic effects, the mass ratio of Cu₂O NPs to Ag must be appropriately balanced. Among the Ag-Cu₂O NPs studied, the CA15 NPs exhibit the highest photocatalytic activity, effectively treating MB solution. Thus, CA15 NPs are selected for further studies.

3.2.2. Effect of Ag-Cu₂O nanocomposite amount on methylene blue treatment

The decomposition of the MB solution occurs directly on the surface of Ag-Cu₂O NPs. Consequently, a larger surface area of Ag-Cu₂O NPs leads to faster MB solution decomposition. The effectiveness of Ag-Cu₂O NPs in treating MB solution largely depends on the amount of NPs used. The treatment efficiency of MB solution with CA15 NPs at various quantities is presented in Table 3.

Table 3 shows that as the amount of Ag-Cu₂O NPs increases, the treatment efficiency of the MB solution also improves. In the dark, the treatment efficiency of MB by CA15 NPs at 0.8 g/L is 5%. This efficiency is primarily due to the adsorption of MB onto the material's surface.

No	Exposure time (hour)	Efficiency of MB degradation by CA15 NPs (%)				
		0.8 g/L	1 g/L	1.2 g/L	1.4 g/L	
1	0 (dark storage)	5.00	9.46	14.25	14.99	
2	2	5.15	11.38	20.90	25.17	
3	4	9.56	15.48	24.53	28.59	
4	6	22.39	27.41	38.53	38.53	
5	8	32.24	35.33	52.13	43.44	
6	10	48.22	57.40	67.90	62.47	
7	12	63.68	69.91	76.83	73.25	

Table 3. Treatment efficiency of MB solution using the CA15 NPs with different amounts.

Increasing the amount of Ag-Cu₂O NPs enhances both adsorption and treatment efficiency. When the CA15 NPs concentration is raised to 1 g/L and 1.2 g/L, the treatment efficiency in the dark increases to 9.46% and 14.25%, respectively. However, at 1.4 g/L, the efficiency only slightly rises to 14.99%. This increase in efficiency with more CA15 NPs is due to a larger contact area between the MB solution and the NPs. Beyond a certain concentration, the dispersion of CA15 NPs in the solution becomes less effective, reducing their ability to form smaller particles and slightly limiting the increase in treatment efficiency.

When illuminated, CA15 NPs decompose the MB solution through photocatalytic degradation, breaking MB molecules into smaller fragments. This process occurs directly on the surface of Ag-Cu₂O NPs. Therefore, increasing the amount of material theoretically increases the surface area and enhances MB treatment efficiency. After 12 hours of UV illumination, the MB treatment efficiency with CA15 NPs at concentrations of 0.8, 1, 1.2, and 1.4 g/L reaches 63.68%, 69.91%, 76.83%, and 73.25%, respectively. Notably, there is minimal difference in efficiency between the 1.2 g/L and 1.4 g/L concentrations. This may be because, at 1.4 g/L, the density of CA15 NPs in the solution is high, affecting their dispersion and making it difficult for them to form smaller particles. Despite increasing the amount of CA15 NPs, the contact area between the NPs and MB solution increases only slightly. Thus, the treatment efficiency with 1.4 g/L CA15 NPs does not surpass that of 1.2 g/L. The relationship between $\ln(C_0/C)$ for MB solutions treated with different concentrations of CA15 NPs and exposure times is shown in Fig. 10.

However, when the CA15 NPs concentration exceeds 1.2 g/L, the degradation rate constant of the MB solution slightly decreases. This occurs because light is scattered, reflected, and absorbed by the CA15 NPs on the surface, preventing it from penetrating deeper into the NPs and thus limiting the enhancement of MB decomposition.

The linear regression coefficients for the degradation of MB solution with different concentrations of CA15 NPs (0.8, 1, and 1.4 g/L) are relatively low, except for the 1.2 g/L concentration. This lower coefficient is due to the MB adsorption on the CA15 NPs surface. However, at 1.2 g/L, the density of CA15 NPs in the solution is sufficient, resulting in a significantly increased MB treatment rate. Consequently, the difference between the photocatalytic process with surface-adsorbed MB and the process without MB is reduced, enhancing the suitability of the linear kinetic model for MB degradation with CA15 NPs at this concentration. Above analysis results indicate

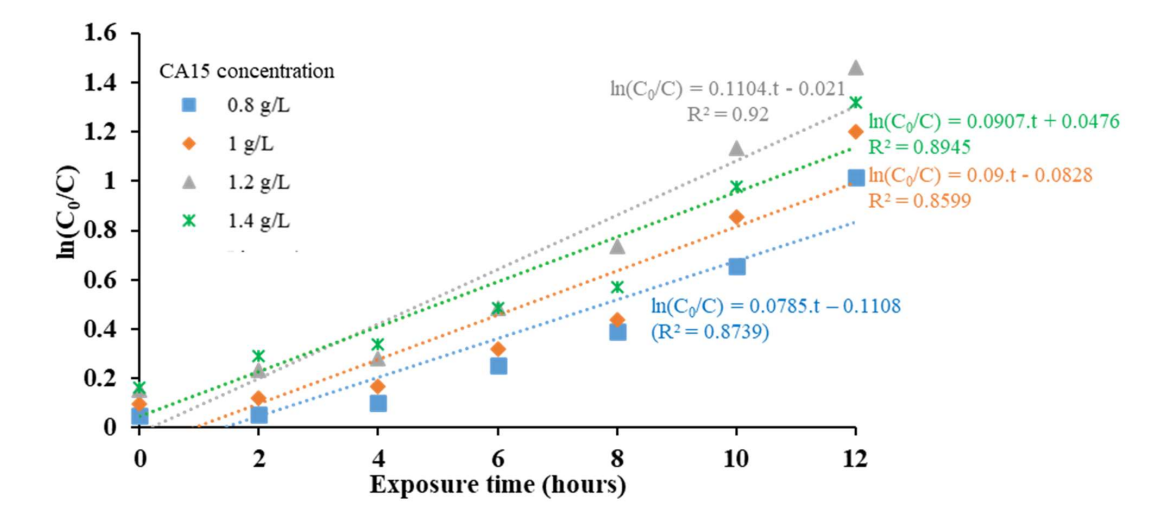


Fig. 10. Relationship between $ln(C_0/C)$ of the MB solution using CA15 NPs with different content and UV exposure times.

that the Ag-modified Cu₂O NPs is effectiveness for treating MB solutions by initial mass ratio of Cu₂O NPs/Ag is 15/1, content of Ag-Cu₂O NPs is 1.2 g/L.

4. Conclusion

Cu₂O NPs were successfully modified with Ag in a single-step process. The AgNPs, with a particle size of 12.68 nm, were evenly dispersed on the Cu₂O NPs surface. After modification, the UV light reflection ability of Cu₂O NPs decreased, and the band gap reduced from 1.81 eV for Cu₂O NPs to 1.58 eV for Ag-Cu₂O NPs. The photocatalytic activity of the Ag-Cu₂O NPs was assessed for methylene blue (MB) degradation. An optimal Cu₂O/Ag mass ratio of 15/1 was identified. At this ratio (CA15 NPs), 76.83% of 6 ppm MB was degraded after 12 hours of UV exposure with a 9 W UV lamp, using a 1.2 g/L dispersion of CA15 NPs in the MB solution.

Acknowledgement

This research is funded by the Vietnam Academy of Science and Technology under grant number NCXS01.05/23-25.

Competing interests

The authors declare no competing interests.

Author statement

Dao Phi Hung: Methodoloy, Nguyen Thuy Chinh: Formal analysis, Supervisor, Nguyen Tien Dung: Investigation, Writing-original draft preparation, Trinh Thanh Huyen: investigation, Vu Dinh Hieu: validation, Thai Hoang: Conceptualization, Funding acquisition, Writing-Reviewing and Editing, Project administration.

Data Availability

The data used to support the findings of this study are included within the article.

References

- [1] S. Ren, M. Du, W. Bu, T. Lin, Assessing the impact of economic growth target constraints on environmental pollution: Does environmental decentralization matter? J. Environ. Manage. 336 (2023) 117618.
- [2] A. Muneeb, M. S. Rafique, M. Ghulam Murtaza, T. Arshad, I. Shahadat, M. Rafique, A. Nazir, Fabrication of Ag-TiO₂ nanocomposite employing dielectric barrier discharge plasma for photodegradation of methylene blue, Phys. B: Condens 665 (2023) 414995.
- [3] S. Liu, Z. Zhang, J. Zhang, G. Qin, E. Zhang, Construction of a TiO₂/Cu₂O multifunctional coating on Ti-Cu alloy and its influence on the cell compatibility and antibacterial properties, Surf. Coat. Technol. 421 (2021) 127438.
- [4] B. C. Silva, K. Irikur, J. B. S. Flor, R. M. M. dos Santos, A. Lachgar, R. C. G. Frem, M. V. B. Zanoni, Electrochemical preparation of Cu/Cu₂O-Cu(BDC) metal-organic framework electrodes for photoelectrocatalytic reduction of CO₂, J. CO₂ Util. 42 (2020) 101299.
- [5] C. Shi, L. Zhang, H. Bian, Z. Shi, J. Ma and Z. Wang, Construction of Ag–ZnO/cellulose nanocomposites via tunable cellulose size for improving photocatalytic performance, J. Clean. Prod. 288 (2021) 125089.
- [6] P. H. Dao, T. D. Nguyen, T. C. Nguyen, A. H. Nguyen, V. P. Mac, H. T. Tran, T. L. Phung, Q. T. Vu, D. H. Vu, T. C. Q. Ngo, M. C. Vu, V. G. Nguyen, D. L. Tran, H. Thai, Assessment of some characteristics, properties of a novel waterborne acrylic coating incorporated TiO₂ nanoparticles modified with silane coupling agent and Ag/Zn zeolite, Prog. Org. Coat. 163 (2022) 106641.
- [7] P. H. Dao, V. T. Trinh, A. H. Nguyen, T. V. Nguyen, T. M. L. Dang, Effects of ZnO nanoparticles and graphene oxide on properties of acrylicpolymernanocomposite coating, Vietnam J. Sci. Tech. 59(3) (2021) 290.
- [8] L. V. A. Sayson and M. D. Regulacio, *Rational Design and Synthesis of Ag@Cu₂O Nanocomposites for SERS Detection, Catalysis, and Antibacterial Applications*, ChemNanoMat, **8** (2022) e202200052.
- [9] Aravind L. Gajengi, Clinton S. Fernandes, Bhalchandra M. Bhanag, Synthesis of Cu₂O/Ag nanocomposite and their catalytic application for the one pot synthesis of substituted pyrrole, Mol. Catal. **451** (2018) 13.
- [10] M. A. Al-Nuaim, A. A. Alwasiti and Z. Y. Shnain, The photocatalytic process in the treatment of polluted water, Chem. Pap. 77 (2023) 677.
- [11] S. Yan, Q. Yue and J. Ma, Rapid fabrication of silver-cuprous oxide core-shell nanowires for visible light photocatalysts, Cryst. Eng. Comm. 23(1) (2021) 24.
- [12] W. Zhang, X. Yang, Q. Zhu, K. Wang, J. Lu, M. Chen & Z. Yang, One-Pot Room Temperature Synthesis of Cu₂O/Ag Composite Nanospheres with Enhanced Visible-Light-Driven Photocatalytic Performance, Ind. Eng. Chem. Res. 53 (2014) 16316.
- [13] H. Qin, Q. Wei, J. Wu, F. Yang, B. Zhou, Y. Wang and S. Tian, Effects of Ag nanoparticles on the visible-light-driven photocatalytic properties of Cu₂O nanocubes, Mater. Chem. Phys. 232 (2019) 240.
- [14] P. H. Dao, H. N. Trinh, T. C. Nguyen, A. H. Nguyen, D. H. Vu, X. T. Nguyen, T. H. G. Hoang, T. D. Nguyen and H. Thai - Enhanced photocatalytic and antibacterial properties of silver–zirconia nanoparticles for environmental pollution treatment, Pure Appl. Chem. 96 (2024) 1117